Cryomilling process of Oxide Dispersion Strengthened CoCrFeMnNi High-Entropy Alloy

SeungHyeok Chung, Ho Jin Ryu *,
Department of Nuclear & Quantum Engineering, Korea Advanced Institute of Science and Technology, 291 Daehakro, Yuseong, 34141, Republic of Korea
**Corresponding author: hojinryu@kaist.ac.kr*

1. Introduction

High Entropy Alloys (HEAs) are promising materials for applications which require the improvements due to its excellent mechanical properties [1]. HEAs have at least 5 elements as the primary elements with an equiatomic concentration range between 5% and 35% [1]. Even though HEAs have excellent mechanical properties, strengthening the material is inevitable to expand the utilization of HEA. Oxide dispersion strengthening (ODS) is effective material strengthening method to use in various fields which have severe environment such as high temperature or high irradiation dose [2]. Dispersing the nano-sized oxide particles within HEAs matrix have been tried since a few years before. However, the researches for ODS-HEAs are very rare. In addition, there are no efforts to investigate the powder before consolidation process as a basic stage. Furthermore, ODS has some issues on commercialization by reason of the difficulty of manufacturing. Dispersing nano-sized oxide particles within matrix homogeneously and reducing the size of oxide particles are very important to improve the performance of ODS [3]. The developing of mechanical alloying (MA) successfully produced ODS steels with dispersed homogeneously nano-sized oxide particles [4].

The aim of this paper is to analyze the Y_2O_3 added CoCrFeMnNi HEA powder by focusing on microstructural changing as milling time increasing. To reduce the size of oxide particles and disperse the nano-sized oxide particles homogeneously much more effectively, cryomilling is selected, which is conducted at liquid nitrogen temperature, instead of room temperature milling. Moreover, milling at cryogenic temperature might prevent the problems occurred during typical room temperature milling and induction melting such as contamination by milling media and compositional segregation. Influence of milling time at a cryogenic temperature on microstructural properties of ODS-HEA powder such as crystallite size and lattice strain were investigated using Scherrer and Halder-Wagner method.

2. Experimental procedures

CoCrFeMnNi HEA powder were manufactured by gas atomization. A mixture of pure elements of Co, Cr, Fe, Mn, and Ni was induction melted under an Ar atmosphere. The delivered molten metal was distributed by high pressured Ar gas and changed into the powder which has different size range. The powder are sieved and separated into different size range from 32 (500 mesh) μm to 2 (10 mesh) mm. The particles which have the size below 32 μm were used for manufacturing the ODS-HEA powder. 0.5wt% of Y_2O_3 was added to form the nano-sized oxide particles. The atomized powder was subsequently cryomilled at -100±10℃ in an Ar atmosphere using stainless steel vessels and balls as grinding media. To lower the temperature to target temperature for cryomilling, liquid nitrogen was injected into the space between the inner vessel and outer vessel. Therefore, the powder in the inner chamber were not contacted with liquid nitrogen. The cryomilling was operated at 200 rpm with a ball-to-powder ratio (BPR) of 10:1. The cryomilling was conducted for 0.5, 1, 2 and 4 hours respectively to investigate the milling time effect on Y_2O_3 added CoCrFeMnNi HEA powder.

The gas-atomized and cryomilled powders were characterized by different methods such as x-ray diffraction (XRD), scanning electron microscopy (SEM), and inductively coupled plasma (ICP). The X-ray diffraction analysis was conducted using an XRD (Rigaku Smartlab) with Cu K_α radiation (λ=0.15406 nm) in θ-2θ configuration. 5°/min for scan speed and 0.01° for step size were used for the measurement. SEM (FEI Magellan400) was used for investigating the surface morphology and structural change of powder as milling time is increasing. To investigate the chemical composition of gas-atomized and as-milled powders, ICP-MS (Agilent ICP-MS 7700S) was used.

3. Result and discussion

3.1 Chemical composition and microstructure

Table I: Chemical composition of the gas-atomized and cryomilled powder

		Chemical composition (wt%)					
		Cr	*Co*	*Fe*	*Mn*	*Ni*	*Y*
Gas-atomized		18.23	18.62	19.98	21.85	21.03	0.29
As-milled	0.5 h	18.05	18.65	19.75	22.17	21.07	0.32
	1 h	18.28	18.32	20.08	21.95	21.08	0.28
	2 h	18.36	18.39	19.91	22.07	21.07	0.20
	4 h	18.30	18.36	19.97	21.80	21.22	0.34

The chemical composition of gas-atomized and cryomilled powder are summarized in Table I. It should be noted that the contents of components were maintained during the cryomilling process. This means Ar atmosphere was preserved well during cryomilling

process so that the oxidation process was suppressed effectively.

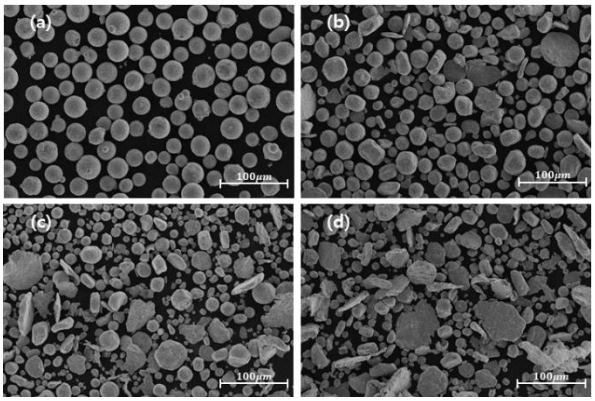

Fig. 1. SEM images of CoCrFeMnNi HEA powder, (a) gas atomized and after milling at -100℃ for (b) 1 h, (c) 2 h, and (d) 4 h

SEM images of CoCrFeMnNi HEA gas-atomized and cryomilled for 1, 2, and 4 h powders are shown in Fig. 1. The gas-atomized powder has fully sphere shape. As the milling time is increasing, the shape of gas-atomized powder was changed into irregular plate shape due to high energy ball during the process. The diameter before milling, gas-atomized powder, has the range of 5-35 μm with a mean diameter of 24 μm. The spherical gas-atomized powder pressed by high energy balls during milling. This process makes powder become brittle due to work hardening [6]. Therefore, the severe stresses are accumulated on the powder and finally the powder is fractured by severe fatigue. The fraction of plate shape particles increases with milling time increasing. Eventually, the spherical shape particles are ground into smaller size particles by high energy ball cryomilling at -100℃.

3.2 X-ray diffraction (XRD) analysis

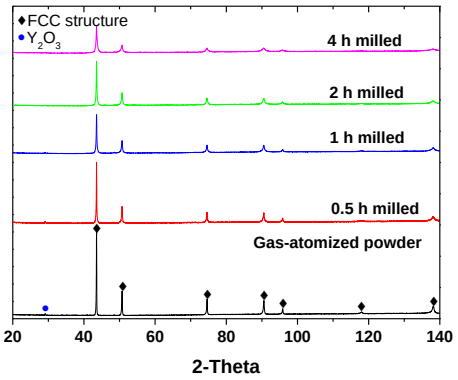

Fig. 2. X-ray diffraction patterns of gas-atomized and cryomilled powder

Fig. 2. shows XRD 2θ pattern results of gas-atomized and cryomilled powders. The peak of Y_2O_3 appears around 2θ = 29° at the XRD patters of gas-atomized powder. The Y_2O_3 peak has faded away after milling started. The phenomena of disappearing Y_2O_3 peak is during milling has been discussed among many researchers so far. Some researchers insist that Y and O are dissociated in metal or dissociated Y and O atoms from Y_2O_3 are dissolved substitutionally and interstitially respectively in the matrix during a milling process [7-9]. However, Dai et al. confirm that Y-O bonding is still remaining in the mixed powder even after being milled for 100 h with XPS analysis [10]. All XRD peaks except the peak from Y_2O_3 are corresponding to FCC structure indicating that no phase transformation occurs during the cryomilling process. However, the intensity of XRD peaks decreases and broadening occurs with increasing of milling time, indicating a refinement of crystallite size and lattice strain increase in the material [5].

3.2.1 Scherrer's method

The crystallite size was estimated by the Scherrer's equation after removing of contributions of instrumental broadening. The crystallite size (D) can be expressed by the following equation [11].

$$D = \frac{K\lambda}{B_D cos\theta} \quad (1)$$

Where λ is the wavelength of Cu K_α radiation (=0.15406 nm), K is the Scherrer constant (=0.9), B is the full width at the half maximum height (FWHM) of $K_{\alpha 1}$ lines. The measured Bragg peaks include the broadening from the instrument. The broadening was adjusted by subtracting the instrumental broadening using a standard material such as LaB_6. The adjusted FWHM is expressed as expressed in equation (2).

$$\beta_D^2 = \beta_{measured}^2 - \beta_{instrumental}^2 \quad (2)$$

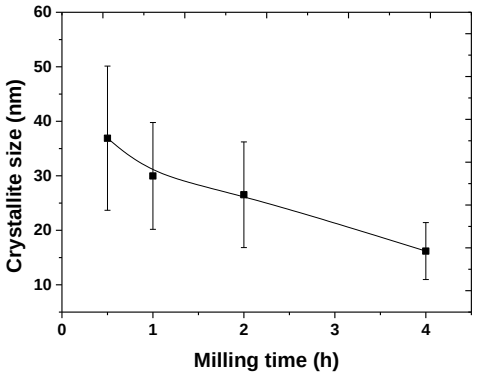

Fig. 3 Changes in FCC crystallite size as a function of milling time

The average crystallite size changes calculated using Scherrer's equation as a function of milling time is shown in Fig. 3. It might have relatively large standard deviation because the calculated crystallite size from

Scherrer's equation is different depending on the lattice plane. The crystallite size of the cryomilled powder is changed from 36.9 nm to 16.2 nm as the milling time increases

3.2.2 Halder-Wagner method

Using Halder-Wagner method, the crystallite size of cryomilled powder was calculated. The Halder-Wagner method shown as following equation [12].

$$\frac{\beta^2}{tan^2\,\theta} = \frac{K\lambda}{D}\frac{\beta}{tan\,\theta\,sin\theta} + 16\epsilon^2 \quad (3)$$

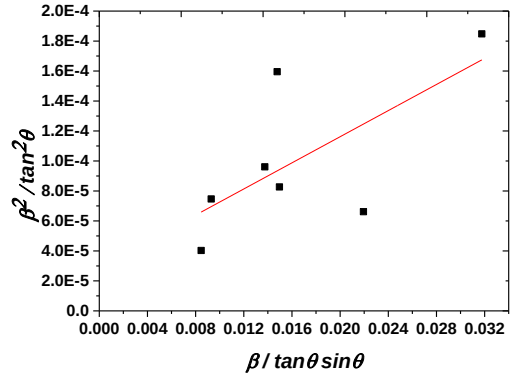

Fig. 4. Halder-Wagner plot of cryomilled for 0.5 h powder

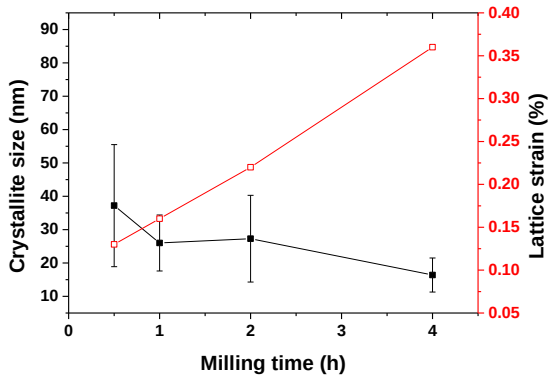

Fig. 5. The variance of crystallite size and lattice strain calculated using Halder-Wagner method as a function of milling time

The equation (3) can be expressed as a straight function of $\beta^2/tan^2\,\theta$ and $\beta/tan\,\theta\,sin\theta$ which has a form of $y = ax + b$. Therefore, the crystallite size D and strain can be obtained from the slope and y-intercept from the straight line. The Halder-Wagner plot of cryomilled for 0.5 h powder is shown in Fig. 4 as an example. The crystallite size in decreasing from 37.2 nm to 16.4 nm. The lattice strain is also changed from 0.13% to 0.36%. It indicates that as milling time increases, crystallite refinement and stress accumulation are progressively occurred. The variation of crystallite size and lattice strain calculated by Halder-Wagner method as a function of milling time is shown in Fig.5. During the milling process in our experiment cases, saturation of crystallite size and lattice strain is not occurred because the strain hardening effect is stronger than recovery. To find the steady state of crystallite and strain, other experiments with longer milling time at cryogenic temperature are necessary.

Table II: The estimated microstructural parameter cryomilled powders

Milling time (h)	Scherrer's method	Halder-Wagner method	
	Crystallite size (D)	Crystallite size (D)	Strain (ϵ)
0.5	36.9	37.2	0.13
1	29.9	26	0.16
2	26.5	27.3	0.22
4	16.2	16.4	0.36

Table II summarizes the microstructural parameters of cryomilled CoCrFeMnNi HEA powder calculated from Scherrer and Halder-Wagner methods. The values of crystallite size from Scherrer and Halder-Wagner methods are almost similar each other. Further studies of microstructural parameters using TEM and EBSD should be done to verify the crystallite size of the powder.

4. Conclusion

The Y_2O_3 added CoCrFeMnNi HEA powder were fabricated and analyzed. The variance of microstructural parameters of powder as a function of milling time was investigated intensively. The crystallite sizes were obtained by Scherrer and Halder-Wagner methods. The lattice strain also evaluated by Halder-Wagner method. The present research has resulted in the following conclusions:

1. The milled powder at cryogenic temperature has almost similar chemical compositions with gas-atomized powder.
2. As the milling time is increasing, the shape of gas-atomized powder was changed into irregular plate shape due to high energy ball during the process.
3. The intensity and broadening have opposite behavior as milling time is increasing. The intensity of XRD peaks decreases with milling time increasing and broadening of XRD peaks occurs with milling time increasing, indicating a refinement of crystallite size and lattice strain increase in the material.
4. The calculated crystallite parameters by Scherrer and Halder-Wagner methods were almost similar. The refinement of crystallite size and stress accumulation continuously occurred.

ACKNOWLEDGMENT

The authors gratefully acknowledge the financial support provided by Agency for Defense Development under the contract 1415156504.

REFERENCES

[1] Zhang, C., Gao, M. C., & Yeh, J.-W. (2016). High-Entropy Alloys: Fundamentals and Applications. High-Entropy Alloys: Fundamentals and Applications. https://doi.org/10.1007/978-3-319-27013-5_12

[2] Toloczko, M. B., Gelles, D. S., Garner, F. A., Kurtz, R. J., & Abe, K. (2004). Irradiation creep and swelling from 400 to 600 ??C of the oxide dispersion strengthened ferritic alloy MA957. Journal of Nuclear Materials, 329–333(1–3 PART A), 352–355. https://doi.org/10.1016/j.jnucmat.2004.04.296

[3] Ukai, S., Mizuta, S., Yoshitake, T., Okuda, T., Fujiwara, M., Hagi, S., & Kobayashi, T. (2000). Tube manufacturing and characterization of oxide dispersion strengthened ferritic steels. Journal of Nuclear Materials, 283–287(PART I), 702–706. https://doi.org/10.1016/S0022-3115(00)00114-8

[4] Zhang, L., Ukai, S., Hoshino, T., Hayashi, S., & Qu, X. (2009). Y2O3 evolution and dispersion refinement in Co-base ODS alloys. Acta Materialia, 57(12), 3671–3682. https://doi.org/10.1016/j.actamat.2009.04.033

[5] Suryanarayana, C., & Norton, M. G. (2013). X-ray diffraction: a practical approach. Springer Science & Business Media.

[6] Xu, H., Lu, Z., Wang, D., & Liu, C. (2016). Microstructural evolution in a new Fe based ODS alloy processed by mechanical alloying. Nuclear Materials and Energy, 7, 1–4. https://doi.org/10.1016/j.nme.2016.04.006

[7] Okuda, T., & Fujiwara, M. (1995). Dispersion behaviour of oxide particles in mechanically alloyed ODS steel. Journal of Materials Science Letters, 14(22), 1600–1603. https://doi.org/10.1007/BF00455428

[8] Ukai, S., & Fujiwara, M. (2002). Perspective of ODS alloys application in nuclear environments . J Nucl Mater 307-Perspective of ODS alloys application in nuclear environments, 311(June), 749–757. https://doi.org/10.1016/S0022-3115(02)01043-7

[9] Kimura, Y., Takaki, S., Suejima, S., Uemori, R., & Tamehiro, H. (1999). Ultra Grain Refining and Decomposition of Oxide during Super-heavy Deformation in Oxide Dispersion Ferritic Stainless Steel Powder. ISIJ International, 39(2), 176–182. https://doi.org/10.2355/isijinternational.39.176

[10] Dai, L., Liu, Y., & Dong, Z. (2012). Size and structure evolution of yttria in ODS ferritic alloy powder during mechanical milling and subsequent annealing. Powder Technology, 217, 281–287. https://doi.org/10.1016/j.powtec.2011.10.039

[11] Scherrer, P. (1918) Bestimmung der Grosse und der Inneren Struktur von Kolloidteilchen Mittels Rontgenstrahlen, Nachrichten von der Gesellschaft der Wissenschaften, Gottingen. Mathematisch-Physikalische Klasse, 2, 98-100

[12] Halder, N. C., & Wagner, C. N. J. (1966). Analysis of the broadening of powder pattern peaks using variance, integral breadth, and Fourier coefficients of the line profile. In Advances in X-ray Analysis (pp. 91-102). Springer, Boston, MA.